Freejet Flows of Gas-Particle Mixtures

R. Ishii* and Y. Umeda†
Kyoto University, Kyoto, Japan

A numerical analysis of freejet flows of gas-particle mixtures is described. A time-dependent technique is applied to solve a two-phase inviscid flow. The piecewise linear interpolation method (PLM) and the method of characteristics (MOC) are used for the gas-phase and the particle-phase flows, respectively. It is found that the effect of the presence of particles on the flow structure is very important.

Nomenclature

C_D = particle drag coefficient
C_p = specific heat at constant pressure
c_f = frozen speed of sound
D = diameter
F = Courant number
L = half-height of nozzle wall at the exit
M = Mach number
N = integration time step
N_u = Nusselt number
P_r = Prandtl number
p = pressure
r_p = particle radius
T = temperature
t = time
u,v = axial and radial velocity, respectively
x,y = axial and radial distance, respectively
γ = ratio of specific heats of gas
ρ = density
ρ_{mp} = material density of particles
ν = loading ratio

Subscripts

g = gas
j = jet
m = Mach disk
S = Stokes flow
O = reservoir
∞ = ambient gas

Superscript

$(^-)$ = dimensional quantity

I. Introduction

THE National Space Development Agency of Japan (NASDA) has a plan to develop a new satellite launcher called H-II. For basic design of this launcher, thermal protection of the rocket wall against strong heating due to thermal radiation from exhausted jet plumes is considered to be very important. Because the thermal emissivity of solid particles is usually much larger than that of gas for typical firing conditions of rocket engines with solid propellant, prediction of the particle-phase flowfield is especially important.[1]

So far, there have been many studies treating supersonic freejet flows.[2-5] General characteristics of supersonic freejet flows are now well understood, at least for dust-free gas jets. The detailed and precise prediction of the flow structure of a freejet flow is, however, very difficult, even numerically. In general, there are many discontinuities in a supersonic freejet flow, among them, shock waves, jet boundaries, and slip lines. Moreover, a new kind of discontinuity appears in the flowfield: the limiting particle streamline that divides the flowfield into dusty and dust-free regions.

When a jet expands into a very rarefied ambient gas or into vacuum space, the transition and the free-molecular flowfields appear downstream of the continuum flowfield. For such a jet, either the continuum or the rarefied gasdynamics must be applied, depending on the characteristics of the flowfield.[6]

In the present paper, the continuum freejet flows are treated by a time-dependent technique. Theoretically, the method of characteristics (MOC) is the most powerful and reliable scheme for the numerical analysis of supersonic flows. For example, Dash and Thorpe used MOC for the analysis of freejet flows in conjunction with a simplifying model for the subsonic flowfield downstream of the Mach disk.[2] Although some of their numerical results have shown fairly good agreement with experiments, the detailed flow structure downstream of the Mach disk may not be predicted accurately by their method.

Here, piecewise linear interpolation method (PLM) is used for the gas-phase flow, and MOC is applied to the particle-phase flow.[7-8] Then, the present numerical scheme is a mixed one. From a numerical point of view, one of the most important difficulties for the analysis of supersonic freejet flows by a time-dependent technique arises from artificially imposed boundary conditions. This is especially the case when a subsonic flow is realized in the region downstream of the Mach disk. It often happens that ill-posed boundary conditions almost invalidate the numerical results. A few types of boundary conditions are tested here.

It is assumed that the jets are exhausted from a uniform sonic nozzle and that the ambient gas pressure is always much lower than the gas pressure at the nozzle exit. Therefore, the jets considered here are the underexpanded ones with Mach disks. Theoretically and numerically, the sonic jet is most difficult to analyze. The present scheme is easily applicable to underexpanded jets with any exit Mach number.

The present numerical calculations were carried out on the supercomputer Fujitsu VP-200 at the Data Processing Center of Kyoto University. The theoretical maximum speed of the VP-200 is about 520 MFLOPS. According to a benchmark test, a sustained speed of the VP-200 is comparable to that of the Cray-XMP.

Presented as Paper AIAA 86-1317 at the AIAA 4th Joint Thermophysics and Heat Transfer Conference, Boston, MA, June 2-4, 1986; received Aug. 22, 1986; revision received April 30, 1987.

*Research Associate, Department of Aeronautics. Member AIAA.
†Research Associate, Department of Aeronautics.

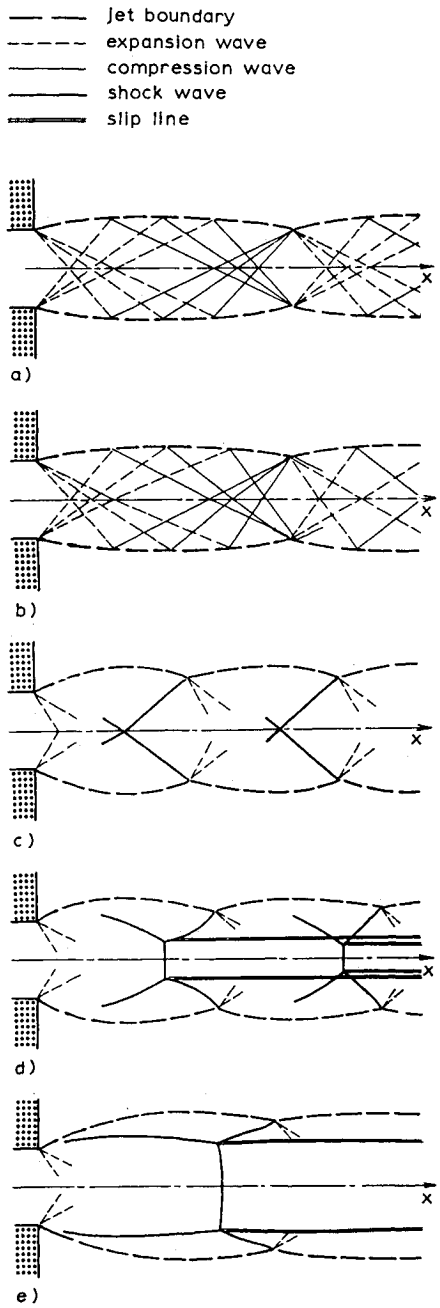

Fig. 1 Flow patterns of underexpanded jets.

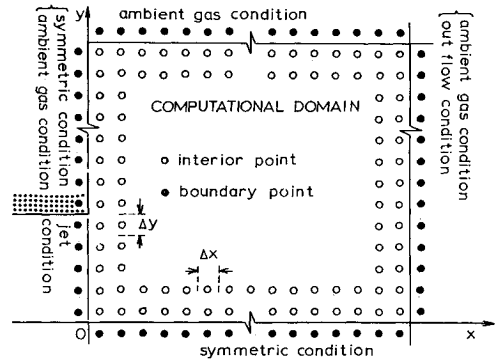

Fig. 2 Grid points and boundary conditions.

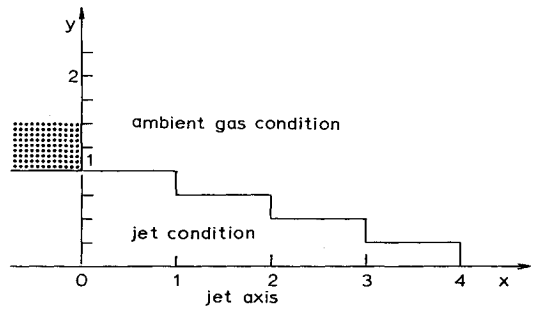

Fig. 3 Initial conditions.

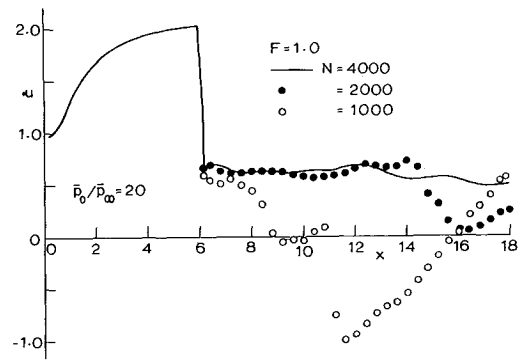

Fig. 4 Convergence history of velocity profile along the jet axis.

II. Basic Equations

Introducing nondimensional quantities by

$$x = \bar{x}/\bar{L}, \quad y = \bar{y}/\bar{L}, \quad t = \bar{c}_{f0}\bar{t}/\bar{L}$$

$$\rho = \bar{\rho}/\bar{\rho}_0, \quad p = \bar{p}/\bar{p}_0, \quad u = \bar{u}/\bar{c}_{f0}, \quad v = \bar{v}/\bar{c}_{f0}$$

$$\bar{T} = \bar{T}/\bar{T}_0, \quad c_f = \bar{c}_f/\bar{c}_{f0}$$

$$\rho_p = \bar{\rho}_p/\bar{\rho}_{p0}, \quad u_p = \bar{u}_p/\bar{c}_{f0}, \quad v_p = \bar{v}_p/\bar{c}_{f0}, \quad T_p = \bar{T}_p/\bar{T}_0 \tag{1}$$

$$A_p = \frac{9}{2\bar{\rho}_{mp}\bar{r}_p^{\,2}}\frac{\bar{L}}{\bar{c}_{f0}}\bar{\mu}f_p, \quad B_p = \frac{3}{\bar{\rho}_{mp}\bar{r}_p^{\,2}P_r}\frac{\bar{C}_{pg}}{\bar{C}_{pp}}\frac{\bar{L}}{\bar{c}_{f0}}\bar{\mu}g_p \tag{2}$$

$$f_p = C_D/C_{D\text{Stokes}}, \quad g_p = N_u/N_{u\text{Stokes}} \tag{3}$$

$$\nu_0 = \bar{\rho}_{p0}/\bar{\rho}_0, \quad \theta = \bar{C}_{pp}/\bar{C}_{pg} \tag{4}$$

the governing equations for an axially symmetric two-phase flow are written in the following forms:

$$\frac{\partial\rho}{\partial t} + \frac{\partial}{\partial x}(\rho u) + \frac{\partial}{\partial y}(\rho v) + \frac{\rho v}{y} = 0 \tag{5}$$

$$\frac{\partial u}{\partial t} + u\frac{\partial u}{\partial x} + v\frac{\partial u}{\partial y} + \frac{1}{\gamma\rho}\frac{\partial p}{\partial x} = -\nu_0 A_p\frac{\rho_p}{\rho}(u - u_p) \tag{6}$$

$$\frac{\partial v}{\partial t} + u\frac{\partial v}{\partial x} + v\frac{\partial v}{\partial y} + \frac{1}{\gamma\rho}\frac{\partial p}{\partial y} = -\nu_0 A_p\frac{\rho_p}{\rho}(v - v_p) \tag{7}$$

$$\frac{\partial p}{\partial t} + u\frac{\partial p}{\partial x} + v\frac{\partial p}{\partial y} - \gamma c_f^{\,2}\left(\frac{\partial\rho}{\partial t} + u\frac{\partial\rho}{\partial x} + v\frac{\partial\rho}{\partial y}\right)$$
$$= \gamma(\gamma-1)\nu_0\rho_p\left\{A_p[(u-u_p)^2 + (v-v_p)^2] - \frac{\theta}{\gamma-1}B_p(T - T_p)\right\} \tag{8}$$

$$p = \rho T \tag{9}$$

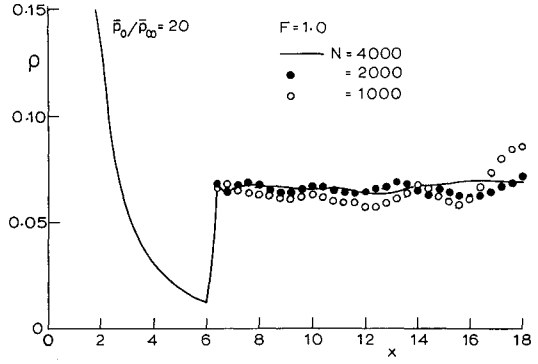

Fig. 5 Convergence history of density profile along the jet axis.

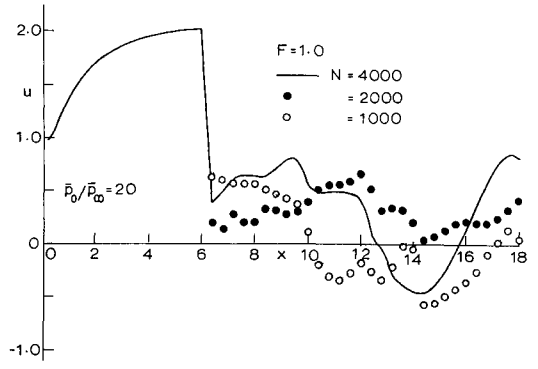

Fig. 6 Convergence history of velocity profile along the jet axis.

$$c_f^2 = p/\rho \tag{10}$$

$$\frac{\partial \rho_p}{\partial t} + \frac{\partial}{\partial x}(\rho_p u_p) + \frac{\partial}{\partial y}(\rho_p v_p) + \frac{\rho_p v_p}{y} = 0 \tag{11}$$

$$\frac{\partial u_p}{\partial t} + u_p \frac{\partial u_p}{\partial x} + v_p \frac{\partial u_p}{\partial y} = A_p(u - u_p) \tag{12}$$

$$\frac{\partial v_p}{\partial t} + u_p \frac{\partial v_p}{\partial x} + v_p \frac{\partial v_p}{\partial y} = A_p(v - v_p) \tag{13}$$

$$\frac{\partial T_p}{\partial t} + u_p \frac{\partial T_p}{\partial x} + v_p \frac{\partial T_p}{\partial y} = B_p(T - T_p) \tag{14}$$

Here the volume fraction of the particles has been neglected. The gas viscosity $\bar{\mu}$ is given by

$$\bar{\mu} = \bar{\mu}_0 (\bar{T}/\bar{T}_0)^\delta \tag{15}$$

where δ is a constant. The particle drag coefficient C_D and the Nusselt number N_u used in the present calculations are, respectively those of Henderson[9] and Carlson and Hoglund.[10]

III. One-Phase Flow

Before proceeding to the analysis of two-phase flows, one-phase (dust-free gas) jets are investigated in detail. Later, the one-phase results will be compared with the two-phase results in order to evaluate the effect of the presence of solid particles on the flow structure of two-phase jets.

Flow Patterns

The expansion of an underexpanded jet into a stagnant ambient gas is characterized by two parameters, M_j and $\bar{p}_j/\bar{p}_\infty$. The former is the flow Mach number at the nozzle exit, and the latter is the ratio of the static pressure of the jet gas at the nozzle exit to the static pressure of the ambient gas. Here

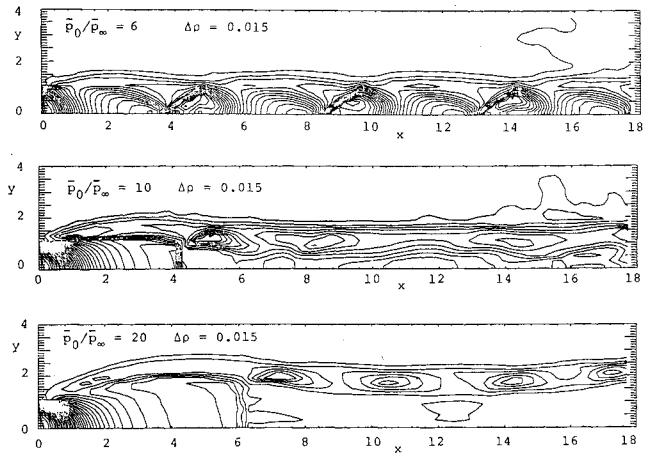

Fig. 7 Density contours.

the pressure at the nozzle exit $\bar{p}_j$ is related with the reservoir pressure $\bar{p}_0$ by an isentropic relation,

$$\bar{p}_j = \bar{p}_0 \left[1 + \frac{\gamma - 1}{2} M_j^2\right]^{-\gamma/(\gamma-1)} \tag{16}$$

Typical flow patterns of axially symmetric supersonic jets expanded into stagnant air are schematically shown in Fig. 1.

In the linearized theory, the flow structure is completely periodic (Fig. 1a). The wavelength $\bar{\lambda}$ of the cell structure is given by

$$\frac{\bar{\lambda}}{2\bar{L}} = \frac{\pi}{\beta_1} \sqrt{M_j^2 - 1} \approx 1.3 \sqrt{M_j^2 - 1} \tag{17}$$

where β_1 is the first zero of the Bessel function of order zero. In the nonlinear theory, however, the flow structure is never completely periodic because shock waves are formed near rear edges of each cell, as shown in Fig. 1b, and the entropy of the gas that flows through the shocks increases. For a larger pressure ratio ($\bar{p}_j/\bar{p}_\infty = 1.5 - 2$ for the uniform sonic jet), cross shocks are formed in the flow nearly periodically (Fig. 1c). When the pressure ratio exceeds some value ($\bar{p}_j/\bar{p}_\infty \approx 2.1$ for the uniform sonic jet), Mach disks are formed nearly periodically in the core region of the jet (Fig. 1d). In such a jet, slip lines appear between flow regions where the gas flows through the Mach disk and the gas flows through the barrel and the reflected shocks. The periodic nature of the core flow becomes weaker with the increasing pressure ratio (Fig. 1e).

Numerical Analysis

The numerical algorithm for the one-phase flow is essentially the same as that proposed by Colella and Glaz.[7] The mesh sizes Δx and Δy are taken to be uniform. The boundary conditions and the grid points are shown in Fig. 2, and the initial conditions in Fig. 3. On the downstream numerical boundary, two types of conditions were tested: the outflow condition,[11-16]

$$\frac{\partial f}{\partial x} = 0, \qquad f = u, v, \rho, p \text{ at } x = 18.2 \tag{18}$$

and the ambient gas condition,

$$f = f_\infty, \qquad f = u, v, \rho, p \text{ at } x = 18.2 \tag{19}$$

For the ambient gas condition, flow conditions at the grid points just inside and outside the downstream boundary become strongly discontinuous. In the PLM scheme, however, the Riemann problem is solved between the states on these two adjacent grid points in order to compute the fluxes on the

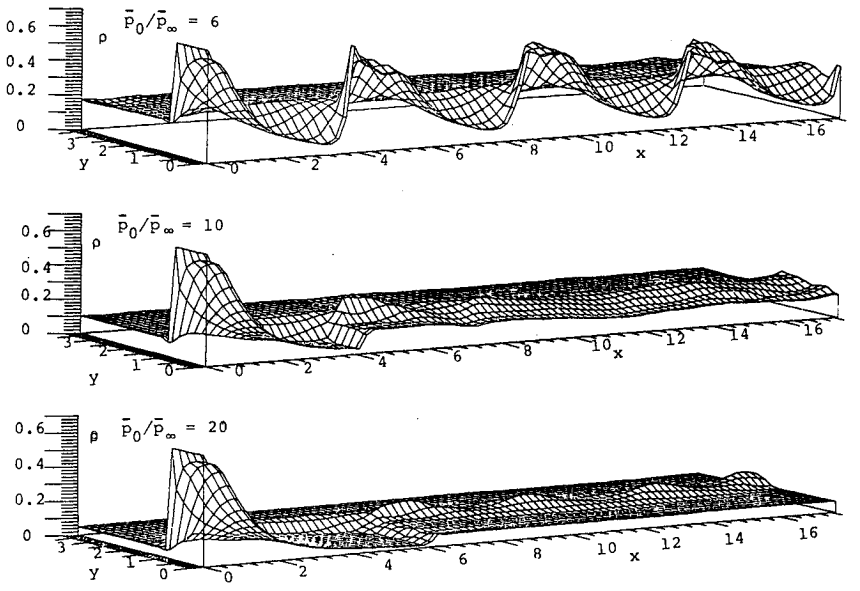

Fig. 8 Perspective views of density distribution.

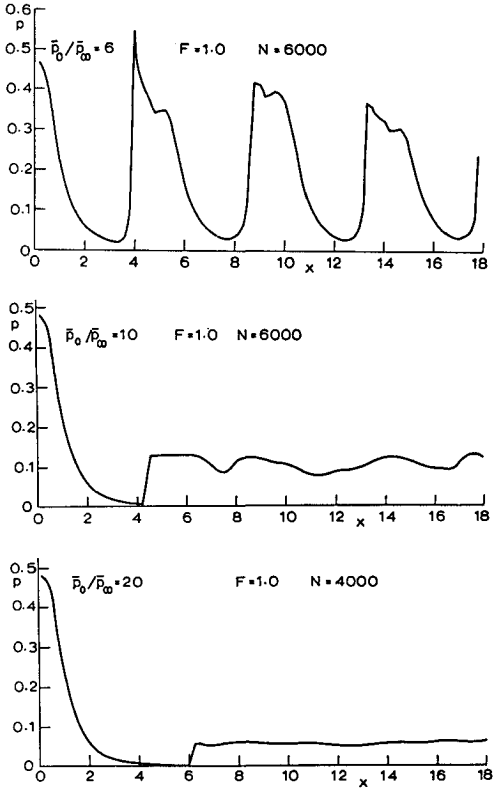

Fig. 9 Distribution of pressure along the jet axis.

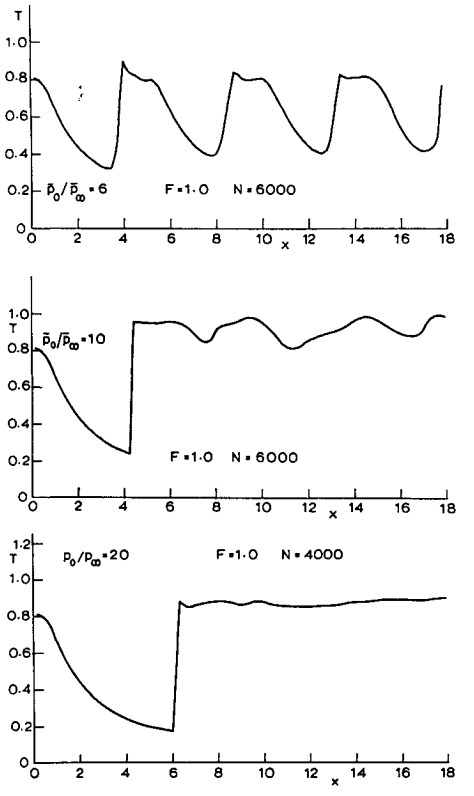

Fig. 10 Distribution of temperature along the jet axis.

downstream boundary. Then, such a specification of the downstream boundary condition does not introduce any numerical difficulty. On the upstream boundary outside the nozzle, the symmetric condition is applied for jets expanded into stagnant air.

The integration time step Δt is given by

$$\Delta t = F \cdot \min \{\sqrt{(\Delta x)^2 + (\Delta y)^2} \Big/ [c_f + \sqrt{u^2 + v^2}]\} \qquad (20)$$

The convergence criteria employed here are

$$\max[|\rho^{N+1} - \rho^N|] \leq 5.0 \times 10^{-3} \qquad (21)$$

and

$$\max[|M^{N+1} - M^N|/M^N] \leq 5.0 \times 10^{-3} \text{ for } M \geq 0.1 \qquad (22)$$

From the present analysis, it has been found that criterion (22) is more severe than criterion (21). Convergence histories of the axial velocity and the axial density profiles along the jet axis are shown in Figs. 4 and 5, respectively. These are for a uniform sonic jet expanded into stagnant air ($\gamma = 1.4$) for $\bar{p}_0/\bar{p}_\infty = 20$ and $\Delta x = \Delta y = 0.2$. Although the criterion given by Eq. (21) was satisfied in the whole computational domain, criterion (22) was applied only in the domain $0 < x < 12$. For $N > 1000$, no flow quantity changed appreciably with time in the region upstream of the Mach disk. In Fig. 6, the

convergence history of the axial velocity along the jet axis is shown for the same jet. In this case, however, the outflow condition, Eq. (18), was applied on the downstream boundary. As is demonstrated in Fig. 6, the axial velocity profile fluctuates with time in the flow region downstream of the Mach disk. Only in the region upstream of the Mach disk, both criteria, Eqs. (21) and (22), were satisfied.

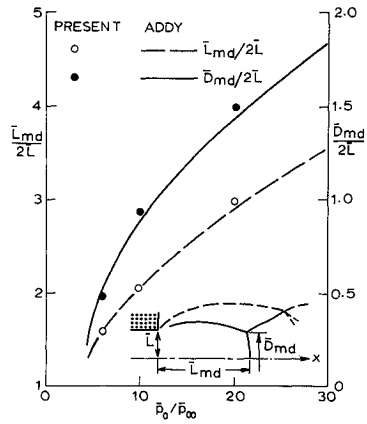

Fig. 11 Comparison of numerical results with experiments.

Here, it is worthwhile to point out that even the results for the condition given by Eq. (19) have not completely converged with time. Although main large-scale flow structures of the jet did not change appreciably for $N > 3000$, they showed a kind of dancing phenomenon about criterion (21). This may imply that the inviscid freejet is essentially unstable. Theoretically, therefore, the steady-state solution may not be realistic, and the fluctuating or the oscillating solution might be essential. In the present paper, however, we consider that the solution closest to a hypothetical steady flow is most preferable.[11]

The downstream and outer boundaries are obviously not physical boundaries but artificially introduced ones. Therefore, the conditions imposed on these numerical boundaries inevitably produce unrealistic disturbances for the main flow in the computational domain. Since the global jet flows toward the downstream boundary, the downstream boundary condition is most critical. The authors have carried out extensive numerical and experimental studies on the one-phase freejets.[16] By detailed comparison of the numerical results with the experiments, we concluded that the ambient gas boundary condition (19) gives the best results for one-phase freejets. Such a boundary condition has also been successfully applied to some problems in astrophysics.[11-15] We will use the ambient gas conditions, Eq. (19), on the downstream boundary and employ convergence criterion (21) in what follows.

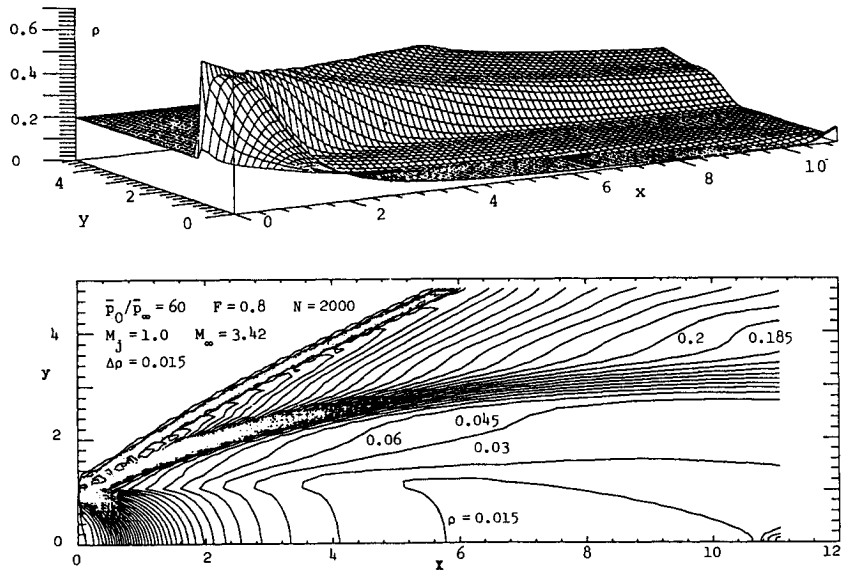

Fig. 12 Perspective view of density distribution and density contours.

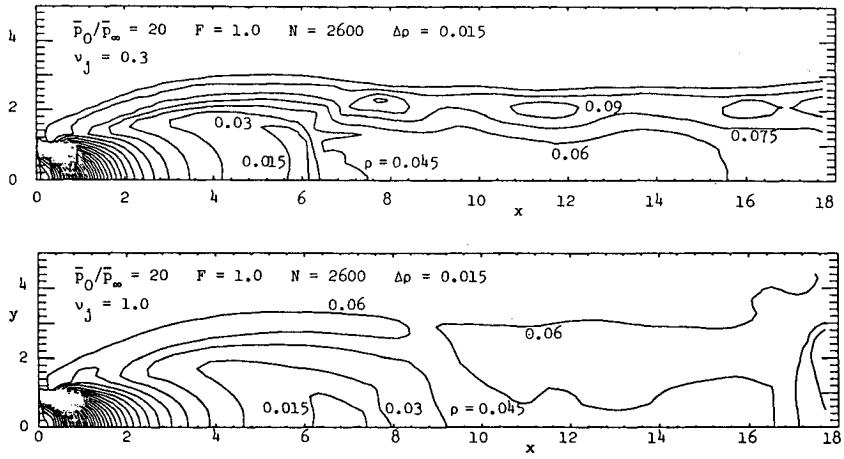

Fig. 13 Density contours of gas phase.

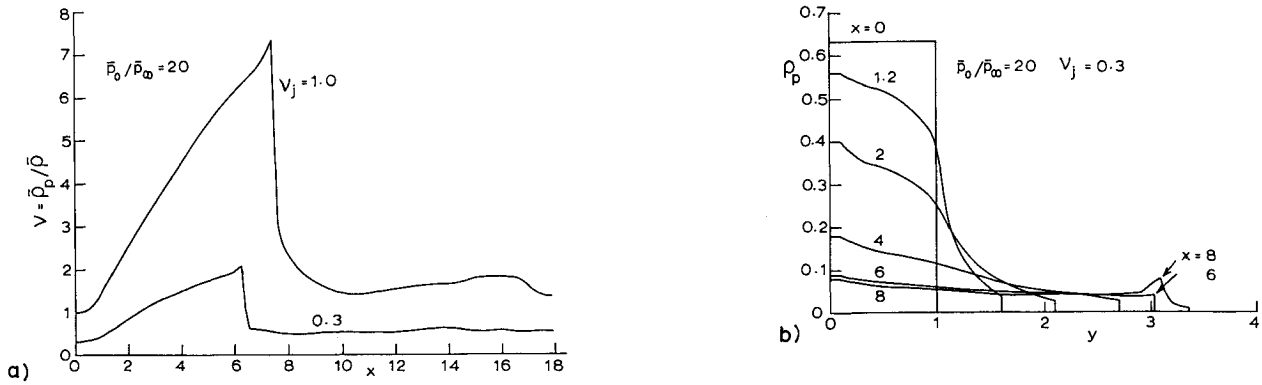

Fig. 14 Particle density and loading radio: a) distribution of local particle loading radio along the jet axis; and b) radial distribution of particle density.

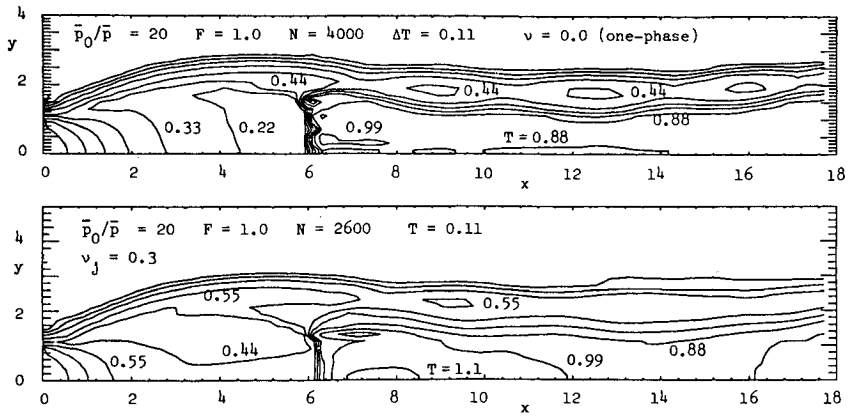

Fig. 15 Temperature contours of gas.

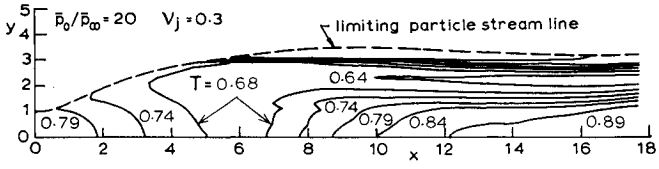

Fig. 16 Temperature contours of particles.

Numerical Results

In Figs. 7 and 8, respectively, the density contours and their three-dimensional surface plots are shown for jets expanded into stagnant air. The results shown in Figs. 9 and 10 are the corresponding distributions of pressure and temperature along the jet axis. Comparing the results for $\bar{p}_0/\bar{p}_\infty = 10$ and 20, we can see that the core flow downstream of the Mach disk for $\bar{p}_0/\bar{p}_\infty = 10$ is more nearly periodic than that for $\bar{p}_0/\bar{p}_\infty = 20$. The most important feature of the freejet flow for a very large pressure ratio is that the flow region downstream of the Mach disk is divided into two subregions by the strong slip lines: one is the core region, where the flow is only slightly periodic, and the other is the outer region surrounded by the jet boundary and the slip line, where the flow is quite highly periodic, perhaps because the pressure waves in the outer region are effectively reflected by the jet boundary and the slip line.

A comparison of the numerical results with the experiments of Ref. 3 is made in Fig. 11. The numerical results of the diameter of the first Mach disk and the distance from the nozzle exit to the Mach disk are shown by solid and open circles, respectively, for the jets expanded into a stagnant gas for pressure ratios 6, 10, and 20. The experimental results of the diameter of the Mach disk and the distance from the nozzle exit to the Mach disk are shown by solid and dotted lines, respectively. As is demonstrated in Fig. 11, the present results agree well with experiments.

When a jet is expanded into an ambient gas that also flows uniformly with a finite velocity, the characteristics of the jet are demonstrated by the five parameters M_j, M_∞, $\bar{p}_j/\bar{p}_\infty$ (or $\bar{p}_0/\bar{p}_\infty$), γ_j, and γ_∞.

Then, the flow structure of the jet will become very complicated. A sample numerical result of a jet immersed in a Mach 3.42 external flow is shown in Fig. 12, where the ambient gas condition was applied on the upstream boundary outside the nozzle. The mesh sizes and the ratios of specific heats are taken to be $\Delta x = \Delta y = 0.125$ and $\gamma_j = \gamma_\infty = 1.4$, respectively. As is well known, an external shock is formed outside the jet boundary. Various types of such jets are now being studied by the present authors, and the results will be reported elsewhere in the near future.

IV. Two-Phase Flow

Aluminum powder is added to many of the solid propellants for rocket motors in order to increase the combustion temperature and the specific impulse. Combustion of such propellants produces aluminum oxide (Al_2O_3) and results in gas-particle flow in the nozzle. Phase nonequilibrium effects in the flow through the nozzle are very important in the rocket nozzle performance. These nonequilibrium effects are also important to determine the fluid dynamic and thermodynamic characteristics of two-phase freejet flows. In the theoretical prediction of intensity of thermal radiation from a two-phase plume, determination of the temperature field of the particle phase is especially important because particle clouds can be very good emitters of thermal radiation.

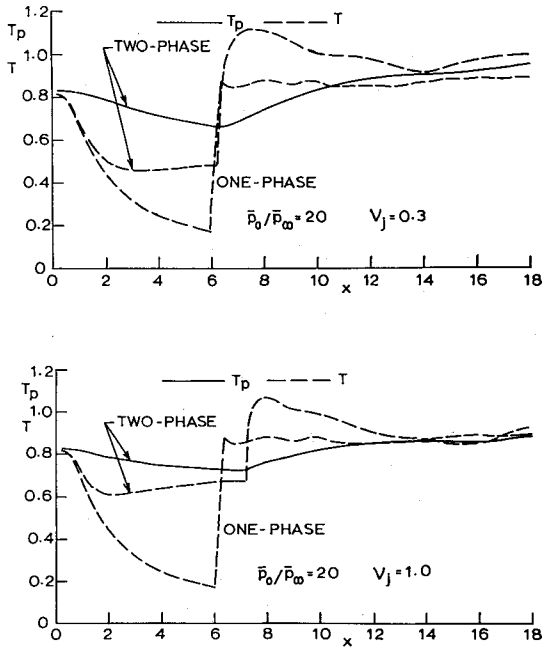

Fig. 17 Temperature distribution along the jet axis.

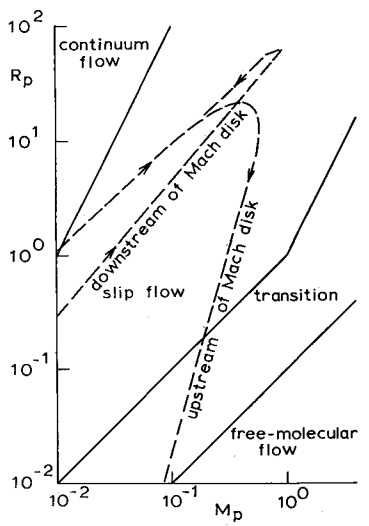

Fig. 18 Particle path in $M_p - R_p$ plane: $\bar{p}_0/\bar{p}_\infty = 20$, $\nu_j = 0.3$.

The gas in a jet for which $\bar{p}_0/\bar{p}_\infty$ (or $\bar{p}_j/\bar{p}_\infty$) $\gg 1$ experiences very rapid and strong expansion and compression. The gas conditions around the solid particles will then change rapidly and strongly. For micron-sized particles in such a flow, inertial, compressibility, and rarefaction effects must be taken into account for the particle drag coefficient C_D and the Nusselt number N_u.

Although, in general, the gas phase and the particle phase are not in equilibrium at the nozzle exit, it is assumed here that the flow is in equilibrium at the nozzle exit. In many practical situations, the velocity and the temperature lags in a nozzle are, at most, about 10% of the absolute gas (or particle) velocity and temperature, respectively. Since, as was stated previously, the gas and particle phases in a jet for $\bar{p}_0/\bar{p}_\infty \gg 1$ become highly unbalanced, the equilibrium assumption of the two phases at the nozzle exit will not lead to appreciable loss of generality in the present analysis.

Numerical Analysis

For the numerical analysis of gas-particle freejet flows, the absolute values of flow quantities at the nozzle exit and the nozzle size are required. The reason for this requirement is that the flow structure of a two-phase jet is characterized not only by the parameters for the one-phase jet but also by the relaxation lengths of the particle velocity and temperature and the particle loading ratio, which depend on the local flow conditions of the gas and particles. Since the equilibrium flow conditions at the nozzle exit are related analytically to the reservoir conditions, the reservoir conditions used in the present calculations are listed in Table 1. In this table, the physical constants of the gas and the particles and the nozzle radius at the exit are also listed. These reservoir conditions are chosen for convenience of comparison of numerical results with experiments, which are now being carried out.

In the calculation U^{N+1}, where U^N are the gas variables at the Nth time step, the particle flowfield is fixed. Next, with the calculated results U^{N+1}, and also U^N and U_p^N, the particle variables U_p^{N+1} are determined by the method of characteristics using the predictor-corrector algorithm given in Ref. 8. Because we are not concerned with transient or time-dependent solutions but only with a converged or time-independent solution, such a procedure will not introduce a serious numerical error. Detailed solution procedure is written in Ref. 17. The particle conditions on the downstream boundary are given by simple linear extrapolations.

Numerical Results

Density contours of the gas are shown in Fig. 13 for $\nu_j = \nu_0 = 0.3$ and 1.0. Comparing these results with the

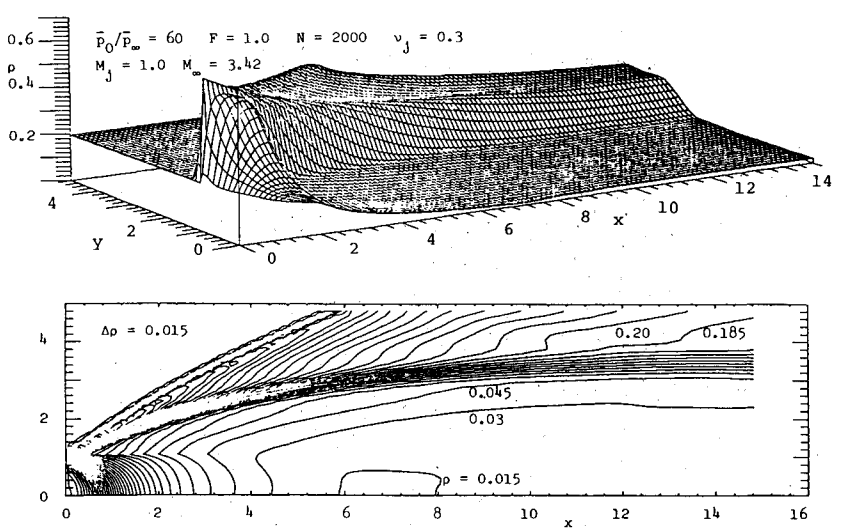

Fig. 19 Perspective view of density distribution of gas and its constant contours.

Table 1 Two-phase jet properties

Reservoir conditions
$\bar{T}_0 = 300$ K
$\bar{\rho}_0 = 3.21$ kg/m^3
$\nu_0 = 0.3, 1.0$
Physical constants
Gas
$\bar{C}_{pg} = 1034$ J/kg.K
$\gamma = 1.4$
$\bar{\mu} = 7.974 \times 10^{-5} (\bar{T}/3200)^{\delta}$ kg/s.m
$P_r = 0.7$
$\delta = 0.6$
Particles
$\bar{C}_{pp} = 1686$ J/kg.K
$\bar{\rho}_{mp} = 3.99 \times 10^3$ kg/m^3
$\bar{r}_p = 2.5$ μm
Nozzle constant
$\bar{L} = 25$ cm

one-phase results, we can find some important features of the gas-particle freejet flow. Some of the important effects of the presence of particles on the flow structure are:

1) The Mach disk is reduced in size and is shifted downstream.

2) The strength of the Mach disk and the barrel shock decreases.

3) The width of the jet boundary increases.

4) The periodic nature of the flow downstream of the Mach disk is weakened appreciably.

5) These trends are enhanced more and more with increasing loading ratio.

In order to investigate the flow characteristics of the two-phase jet in more detail, the local loading ratio ν ($= \nu_j \rho_p / \rho$) along the jet axis and the radial distribution of the particle density are shown in Fig. 14. In Fig. 14a, it can be seen that the local loading ratio ν becomes very large (several times as large as that at the nozzle exit) in the expansion region upstream of the Mach disk. This indicates that the effect of the presence of particles on the core flow of the jet will be very important, even when the loading ratio at the nozzle exit is small. Moreover, as is shown in Fig. 14b, the particle density is largest near the jet axis in the flow region upstream of the Mach disk. These facts will suggest that the characteristics of the Mach disk will be strongly affected by the presence of particles.

Temperature contours of the gas and particles are shown in Figs. 15 and 16, respectively. The temperature distributions along the jet axis are shown in Fig. 17. These results show that the gas temperature in the two-phase jet is appreciably different from the corresponding one-phase result.

Next, the particle conditions in the jet are investigated. We denote the particle Mach number and the particle Reynolds number, respectively, by

$$M_p = \frac{|\bar{u} - \bar{u}_p|}{\bar{c}_f}, \qquad R_p = \frac{2\bar{r}_p \bar{\rho} |\bar{u} - \bar{u}_p|}{\bar{\mu}} \tag{23}$$

where $\bar{u}$ and $\bar{u}_p$ are the velocity vectors of the gas and the particles, respectively. The gas conditions around the particles along the jet axis are represented in the $M_p - R_p$ plane as in Fig. 18, which indicates that the inertial, compressibility, and rarefaction effects are important in the description of gas-particle interactions, depending on location in the jet.

Finally, a two-phase jet expanded into $M = 3.42$ ambient air flowing uniformly is shown in Fig. 19, where the reservoir conditions are set to be $\bar{T}_0 = 3200$ K and $\bar{\rho}_0 = 3.21$ kg/m^3. It is interesting that the Mach disk is not present in the jet. The flow structure is very different from the jet expanded into stagnant air. For such a jet, systematic calculations are now being carried out, and the results will be reported in the near future.

V. Conclusions

A numerical analysis of gas-particle freejet flows was carried out. The numerical results have shown that the effect of particles on the jet structure is very important. Since the particle phase cannot be expanded as effectively as the gas phase, the local particle loading ratio becomes very large in the core region of the jet, especially in front of the Mach disk. Then, the characteristics of the Mach disk are very much affected by the presence of particles. The Mach disk is reduced in size and strength, and the shock cell structure becomes less periodic. In a dust-free jet, the Mach disk is nearly plane but, in the two-phase jet, it is very concave.

In general, the Mach disk shock is the strongest of the shocks produced in the flowfield of a jet. The characteristics of the Mach disk are therefore very important for the flow structure downstream of the Mach disk. In the two-phase jet, the presence of particles is most critical for determining the characteristics of the Mach disk. Such a situation suggests that the flow structure of the two-phase jet is much different from that of the dust-free jet.

References

[1]Buckley, F.T. Jr., "Radiation-Resisted Shock Waves in Gas-Particle Flows," *AIAA Journal,* Vol. 9, Aug. 1971, pp. 1603–1607.

[2]Dash, S.M. and Thorpe, R.D., "Shock-Capturing Method of One- and Two-Phase Supersonic Exhausted Flow," *AIAA Journal,* Vol. 19, July 1981, pp. 842–851.

[3]Addy, A.L., "Effect of Axisymmetric Sonic Nozzle Geometry on Mach Disk Characteristics," *AIAA Journal,* Vol. 19, Jan. 1981, pp. 121–122.

[4]Reis, R.J., Aucoin, P.J., and Stechan, R.C., "Prediction of Rocket Exhausted Flowfields," *AIAA Journal,* Vol. 17, Feb. 1979, pp. 155–159.

[5]Muntz, E.P., Hamel, B.B., and Maguire, B.L., "Some Characteristics of Exhausted Plume Rarefraction," *AIAA Journal,* Vol. 8, Sept. 1970, pp. 1651–1658.

[6]Ashkenas, H. and Sherman, F.S., "The Structure and Utilization of Supersonic Free-Jets in Low Density Wind Tunnels," *Rarefied Gas Dynamics,* Vol. 2, edited by J.H. de Leeuw, Academic Press, Orlando, FL, 1965, pp. 84–105.

[7]Colella, P. and Glaz, H.M., "Efficient Solution Algorithm for the Riemann Problem for Real Gases," Rept. No. 15776, Lawrence Berkeley Laboratory, 1983.

[8]Zucrow, M.J. and Hoffman, J.P., *Gas Dynamics,* Vol. II, Wiley, New York, 1977.

[9]Henderson, C.B., "Drag Coefficient of Spheres in Continuum and Rarefied Flows," *AIAA Journal,* Vol. 14, June 1976, pp. 269–277.

[10]Carlson, D.J. and Hoglund, R.F., "Particle Drag and Heat Transfer in Rocket Nozzle," *AIAA Journal,* Vol. 11, Feb. 1973, pp. 1980–1981.

[11]Sawada, K., Shima, E., Matsuda, T., and Inaguchi, T., "The Osher Upwind Scheme and Its Application to Cosmic Gas Dynamics," *Memoirs of Faculty of Engineering,* Kyoto Univ., Vol. 48, No. 2, 1986, pp. 240–264.

[12]Shima, E., Matsuda, T., Takeda, H., and Sawada, K., "Hydrodynamic Calculation of Axisymmetric Accretion Flow, " *Monthly Notices of the Royal Astronomical Society,* Vol. 217, Nov. 1985, pp. 367–386.

[13]Sawada, K., Matsuda, K., and Hachisu, I., "Spiral Shocks on a Roche Lobe Overflow in a Semi-detached Binary System," *Monthly Notices of the Royal Astronomical Society,* Vol. 219, March 1986, pp. 75–88.

[14]Sawada, K., Matsuda, T., and Hachisu, I., "Accretion Shocks in a Close Binary System," *Monthly Notices of the Royal Astronomical Society,* Vol. 221, Aug. 1986, pp. 679–687.

[15]Shima, E., Matsuda, T., and Inaguchi, T., "Interaction Between a Stellar Wind and an Accretion Flow," *Monthly Notices of the Royal Astronomical Society,* Vol. 221, Aug. 1986, pp. 687–706.

[16]Matsuda, T., Umeda, Y., Ishii, R., Yasuda, A., and Sawada, K., "Numerical and Experimental Studies on Choked Underexpanded Jets," AIAA Paper 87-1378, June 1987.

[17]Ishii, R. and Umeda, Y., "Nozzle Flows of Gas-Particle Mixtures," *Physics of Fluids,* Vol. 30, No. 3, 1987, pp. 752-760.